

Vincent T. Wood

NOAA/OAR/National Severe Storms Laboratory, Norman, Oklahoma

1. INTRODUCTION

On the afternoon of Monday, 20 May 2013, a tornado touched down west of Newcastle, Oklahoma at 1956 UTC, rapidly intensifying and attaining EF4 intensity within 3 minutes and about 1 km from touchdown. The tornado stayed on the ground for approximately 40 minutes over a 22-km path (Fig. 1), tearing through a heavily populated section of Moore, Oklahoma, killing 23 people and injuring scores more. Between 2016 and 2018 UTC, the EF5 tornado was at its maximum intensity as it moved across Moore. After 2018 UTC, it shrank in size, with damage decreasing from EF5- to EF2-scale before becoming a thin rope tornado. The tornado eventually dissipated near Lake Stanley Draper around 2035 UTC. This information was based on the combined reports of Norman NWSFO, the city of Moore and Cleveland county emergency management officials, the National Weather Center damage survey teams, media, *Storm Data* and other sources. The 20 May 2013 tornado followed a track roughly similar to the Bridge Creek-Moore tornado of 3 May 1999 (Burgess et al. 2002).

This paper describes the evolution of the Newcastle-Moore, Oklahoma tornado as detected by the Oklahoma City, Oklahoma Terminal Doppler Weather Radar (TOKC). The objectives of the paper are twofold: (a) to provide detailed information on the high-resolution Doppler velocity fields in and around the tornado, and (b) to compare estimates of tornado rotational velocity and core diameter with the tornado damage track in terms of the Enhanced Fujita (EF) scale rating (McDonald et al. 2004; WSEC 2006).

2. DATA SOURCES

Operated by the Federal Aviation Administration, TOKC is a C-band Doppler weather radar located in the northwest section of Norman, Oklahoma (Fig. 1). The location of the radar gave it an excellent vantage point from which to observe the tornado, which was within 15 km of TOKC for its entire lifetime. As the Newcastle-Moore tornado made its closest approach (5.4 km) to TOKC at 2017 UTC, data were collected at heights as low as ~50 m AGL. Radar characteristics are shown in Table 1.

TOKC data were processed between 1901 and 2100 UTC, thus providing excellent radar data that were continuous during the tornado's life. For data editing, the Solo3 radar data editing software, now in its third version (<https://www.eol.ucar.edu/software/solo3>), was used (Oye

et al. 1995). One of the limitations of the TOKC is that the Nyquist velocity is only 16 m s^{-1} (Table 1), causing multiple folds in the data where there are high velocities in the vortex signature, making it sometimes difficult to dealias the velocities properly. Time continuity of vortex signatures including calculated Doppler rotational velocities and core diameters between volume scans was necessitated to ensure that the signatures did not change drastically and unrealistically.

TABLE 1. TOKC operating characteristics.

| | |
|------------------------|--|
| Wavelength | 5 cm |
| Transmitted Peak Power | 250 kW |
| Half-power Beamwidth | 0.55° |
| Effective Beamwidth | 1.2° |
| Nyquist Velocity | $16 \text{ to } 22.5 \text{ m s}^{-1}$ |
| Frequency | 5.6 to 5.65 GHz |
| Range Gate Spacing | 150 m |
| Azimuthal Gate Spacing | 1.0° |
| Lowest Elevation Angle | 0.5° |
| Polarization | Linear Horizontal |
| Sensitivity | Similar to WSR-88D |
| Clutter Filter | Aggressive |

TOKC data were collected at uniform range and azimuth, but were not uniformly distributed in space and, more importantly, were not distributed in horizontal or vertical planes that the meteorologist chooses. A two-dimensional contouring technique of Bourke (1987) was used to display data in a Cartesian coordinate system. Because we wanted to produce the contours in a radar coordinate system (range, azimuth and elevation grids) without altering the gridded data, we modified the technique to display data in this system in order to retain peak Doppler velocity values that would have been lost if using an objective analysis scheme. If an objective analysis scheme were applied to the TOKC data, the interpolated grid point value at a peak would have been strongly influenced by nearby data values, blunting the peaks, while the lesser influence of more distant values would serve to smooth or filter out small-scale meteorological noise. This could lead to misinterpretation of data analysis. Fig. 2 provides an example of the modified Bourke technique, exhibiting the contours of the high-resolution Doppler velocity values in gridded range and azimuth coordinates at lowest elevation angle of 0.5° . An advantage of the technique is that the high-resolution TOKC data, particularly extreme velocity values, remain unaltered, thus preserving the values within and surrounding the vortex signature before meteorological analysis and interpretation proceed.

Damage survey methodology (Ortega et al. 2014) and the application of the NWS damage assessment toolkit (Camp et al. 2014) for the Newcastle-Moore, Oklahoma tornado of 20 May 2013 were described

Corresponding author address: Vincent T. Wood, National Severe Storms Laboratory, 120 David L. Boren Blvd., Norman, OK 73072; e-mail: Vincent.Wood@noaa.gov

elsewhere in this volume, and will not be discussed here due to limited space. Detailed information on the evolution of high-resolution Doppler velocity fields in and around the tornado at proximity to TOKC is discussed in the subsequent section.

3. DOPPLER ROTATIONAL VELOCITY AND CORE DIAMETER PARAMETERS

The rotational velocity (V_{ROT}) is $\Delta V/2=(V_{MAX}-V_{MIN})/2$, which is calculated as the average of extreme positive (V_{MAX}) and negative (V_{MIN}) Doppler velocity values across an estimated tornado core diameter (CD). The estimates of V_{ROT} and CD are compared with tornado damage track to determine any relationship between the tornado's varying core size and strength and the ground damage path, as will be shown in the subsequent section.

4. PRELIMINARY RESULTS

Figures 3-9 reveal the presence of a *tornado signature* (TS), whereas Fig. 10 presents the appearance of a *tornadic vortex signature* (TVS). The TS is a vortex signature of extreme Doppler velocity values (of opposite sign) separated by a few beamwidths in the azimuthal direction. A TS arises when the tornado is within a few kilometers of a radar and the tornado is larger than the radar beam (Brown et al. 1978; Brown 1998). In contrast, the TVS arises when a vortex signature of degraded Doppler velocity extremes (of opposite) is separated by about one beamwidth in the azimuthal direction, and the radar beam is wider than the tornado (Brown et al. 1978). The characteristics of the tornado are degraded to such an extent that neither the size nor strength of the tornado may be recoverable. Additionally, the TVS is unaffected by whether the tornado structure consists of one or two cells (Wood and Brown 2011).

The high-resolution Doppler velocity data gathered from lowest-elevation (0.5°) scans are compared to ground damage survey EF scale estimates (Figs. 3-10). Most Doppler velocity peaks (green X's) are not at the same range from TOKC because target motion in the tornado vortex is slightly divergent as a result of debris and precipitation centrifuging (Dowell et al. 2005). Fig. 6 (Fig. 7) shows a slightly convergent vortex signature in spite of the fact that the Doppler velocity peaks are approximately (not) at the same range from TOKC.

TOKC measured the strongest rotational velocities exceeding 75 m s^{-1} in the lowest 50 m AGL (Figs. 6 and 11) when the tornado was closest (5.4 km) to the radar at 2017 UTC.¹ After 2018 UTC, the tornado began to shrink in size, reducing from EF5- to EF2-damage (Figs. 7-10) before eventually dissipating. A compact swath of EF5 damage a few hundred meters west of Interstate

¹Although this peak in V_{ROT} corresponds to a swath of EF5 damage in the survey (Figs. 1 and 6), it has since been determined by civil engineers that the school building used as the primary EF5 damage indicator suffered from substandard construction, and this swath will likely be reduced to EF4 in a future revision to the damage survey (D. Burgess, personal comm.).

Highway 35 in Moore, which occurred at around 2023 UTC as V_{ROT} was decreasing rapidly (Fig. 11), can be explained by the slowing of the tornado's ground-relative speed as it traced out a very small loop in its path (the cusp in the damage track in Fig. 2).

The tornado vortex's CD (black circle in Figs. 3-10) and rotational velocity may correspond to the width of the ground damage path. For example, the core diameter at which most damaging winds occur may increase the damage path width at one time (Fig. 4) and decrease the width at another time (Fig. 5). Evolution of estimated rotational velocity and core diameter in relation to the varying EF ratings is presented in Fig. 11, although the varying width of the path is not shown. It can be seen that, during its intensification phase (1956-2017 UTC), V_{ROT} and CD were inversely related; i.e. the vortex contracted as the winds increased. After peak intensity, both V_{ROT} and CD trended downward as the tornado began to decay (2017-2036 UTC). Similar trends were inferred from other mobile Doppler radar observations of tornadoes taken at comparable heights (Tanamachi et al. 2013; their Table 1).

Most of the time, the center of the Doppler velocity signature tracked a few hundred meters farther north than the centerline of the damage survey due to stronger winds on the south side of the tornado resulting from the added translational motion (toward the east-northeast) of the tornado (Figs. 4-10). This is consistent with the findings of Wurman and Alexander (2005) and Bodine et al. (2013) that the significant tornado ground damage occurs along the right side of the tornado relative to its translational motion, where wind speeds are enhanced by storm motion. At 1956 UTC, the center of the Doppler velocity signature was coincident with tornado touchdown (Fig. 3).

5. CONCLUSIONS AND FUTURE WORK

The Newcastle-Moore, Oklahoma tornado of 20 May 2013 afforded the opportunity to (a) document detailed information on the evolution of high-resolution Doppler velocity fields in and around the tornado at close proximity to TOKC, and (b) implement comparisons between a damage survey and Doppler velocity measurements. This preliminary study is part of our ongoing research to continue documentation of detailed information on the evolution of the high-resolution Doppler velocity and reflectivity fields surrounding the tornado at all elevation angles, before conclusions will be emerging.

6. ACKNOWLEDGMENTS

The author appreciates the helpful comments on this manuscript provided by Robin Tanamachi and Rodger Brown of NSSL. Discussion with Rodger Brown, Don Burgess, Pam Heinselman, Robin Tanamachi, and others were also helpful in this analysis. John Cho, TDWR engineer, is acknowledged for providing the effective beamwidth (Table 1). The author would like to thank numerous people at the National Weather Center who

tirelessly contributed to the tornado ground damage survey of 20 May 2013.

Center Tech. Rep., Texas Tech University, 15 pp + 3 appendices. [Available online at <http://www.depts.ttu.edu/nwi/Pubs/FScale/EFScale.pdf>]

7. REFERENCES

- Bourke, P., 1987: CONREC – A Contouring Subroutine. [Available online at <http://paulbourke.net/papers/conrec/>]
- Brown, R. A., 1998: Nomogram for aiding the interpretation of tornadic vortex signatures measured by Doppler radar. *Wea. Forecasting*, **13**, 505-512.
- _____, L. R. Lemon, and D. W. Burgess, 1978: Tornado detection by pulsed Doppler radar. *Mon. Wea. Rev.*, **106**, 29-38.
- Burgess, D. W., M. A. Magsig, J. Wurman, D. C. Dowell, and Y. Richardson, 2002: Radar observations of the 3 May 1999 Oklahoma City tornado. *Wea. Forecasting*, **17**, 456-471.
- Camp, J. P., L. P. Rothfusz, A. Anderson, D. Speheger, K. L. Ortega, and B. R. Smith, 2014: Assessing the Moore, Oklahoma (2013) tornado using the National Weather Service damage assessment toolkit. Extended Abstract, *The Special Symposium on Severe Local Storms: The Current State of the Science and Understanding Impacts*. 5 February, Atlanta, Amer. Meteor. Soc., Boston, P830.
- Dowell, D. C., C. R. Alexander, J. M. Wurman, and L. J. Wicker, 2005: Centrifuging of hydrometeors and debris in tornadoes: Radar-reflectivity patterns and wind-measurement errors. *Mon. Wea. Rev.*, **133**, 1501-1524.
- McDonald, J. R., G. S. Forbes, and T. P. Marshall, 2004: The enhanced Fujita (EF) scale. Preprints, *22nd Conf. on Severe Local Storms*, Hyannis, MA, Amer. Meteor. Soc., 3B.2. [Available online at <http://ams.confex.com/ams/pdfpapers/81090.pdf>]
- Ortega, K. L., D. W. Burgess, G. S. Garfield, C. Karstens, J. G. LaDue, T. P. Marshall, T. C. Meyer, B. R. Smith, R. Smith, D. Speheger, and G. J. Stumpf, 2014: Damage survey and analysis of the 20 May 2013 Newcastle-Moore, OK EF-5 tornado. Extended Abstract, *The Special Symposium on Severe Local Storms: The Current State of the Science and Understanding Impacts*. 5 February, Atlanta, Amer. Meteor. Soc., Boston, P828.
- Oye, R., C. Mueller, and S. Smith, 1995: Software for radar translation, visualization, editing, and interpolation. Preprints, *27th Conf. on Radar Meteorology*, Vail, Colorado, Amer. Meteor. Soc., 359 - 361.
- Tanamachi, R. L., H. B. Bluestein, M. Xue, W.-C. Lee, K. A. Orzel, S. J. Frasier, and R. M. Wakimoto, 2013: Near-surface vortex structures in a tornado and a sub-tornado-strength, convective-storm vortex observed by a mobile, W-band radar during VORTEX2. *Mon. Wea. Rev.*, **141**, 3661-3690.
- Wood, V. T., and R. A. Brown, 2011: Simulated tornado vortex signatures of tornado-like vortices having one- and two-celled structures. *J. Appl. Meteor. Climatol.*, **50**, 2338-2342.
- WSEC, 2006: A recommendation for an enhanced Fujita scale (EF-scale). Wind Science and Engineering

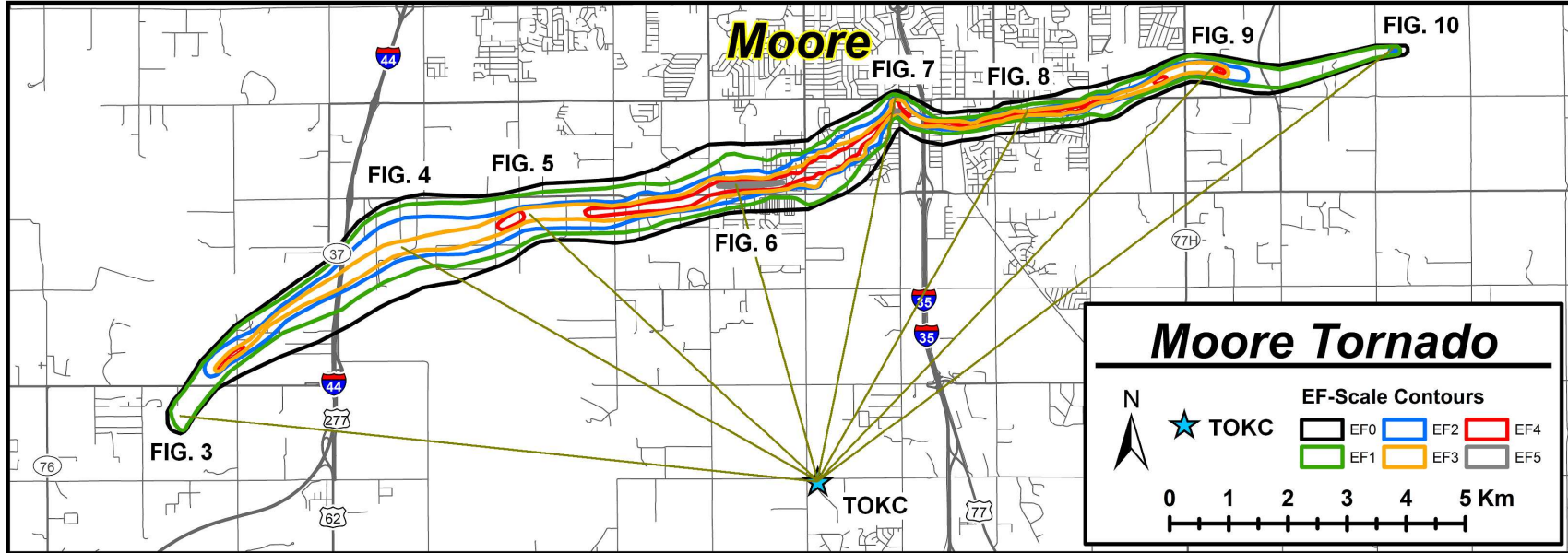


FIG. 1. Damage survey compiled by the National Weather Center teams for the Moore, Oklahoma tornado of 20 May 2013. The EF-ratings along the damage path are contoured according to different colors. The blue star shows the location of TOKC. The radial distances (R_c) from TOKC to the center grids of Doppler velocity patterns superimposed on colored, contoured damage (EF-ratings) paths are indicated in the upper part of Figs. 3-10.

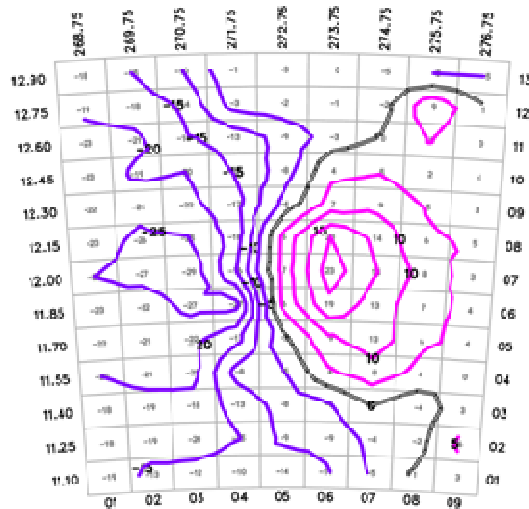


FIG. 2. Gridded Doppler velocity values ($m s^{-1}$) at the 0.5°-elevation angle. Pink (magenta) contours, respectively, represent positive (negative) ground-relative Doppler velocities – flow away from (toward) the radar. Zero Doppler velocity represents flow perpendicular to the radar viewing direction, as indicated by the gray contour. A contour interval of $5 m s^{-1}$ is indicated. Range (km), azimuth (degree), range and azimuth cell numbers are indicated.

20130520 $R_c = 10.8$ km, $AZ_c = 275.8^\circ$, $EL = 0.50^\circ$, $Z_c = 0.102$ km
 1955:57 UTC EFO E F2 E F4
 $V_{rot} = 28$ m s⁻¹ EF1 EF3 EF5
 $CD = 585$ m $V_{min} = -36$ $V_{max} = 20$

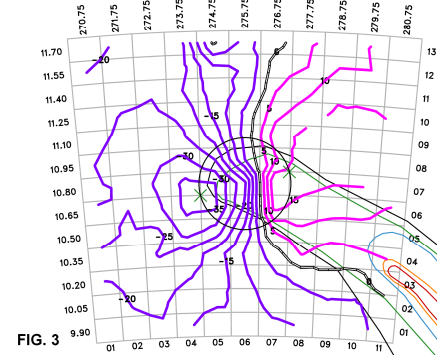


FIG. 3

20130520 $R_c = 8.1$ km, $AZ_c = 300.8^\circ$, $EL = 0.50^\circ$, $Z_c = 0.074$ km
 2005:53 UTC EFO E F2 E F4
 $V_{rot} = 44$ m s⁻¹ EF1 EF3 EF5
 $CD = 881$ m $V_{min} = -53$ $V_{max} = 35$

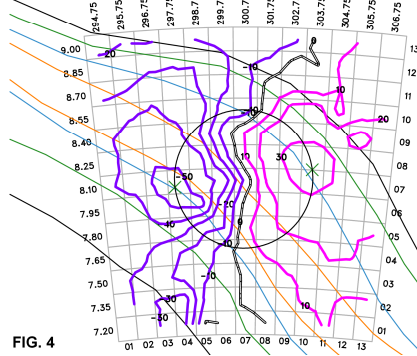


FIG. 4

20130520 $R_c = 6.8$ km, $AZ_c = 312.8^\circ$, $EL = 0.50^\circ$, $Z_c = 0.062$ km
 2009:58 UTC EFO E F2 E F4
 $V_{rot} = 66$ m s⁻¹ EF1 EF3 EF5
 $CD = 388$ m $V_{min} = -79$ $V_{max} = 56$

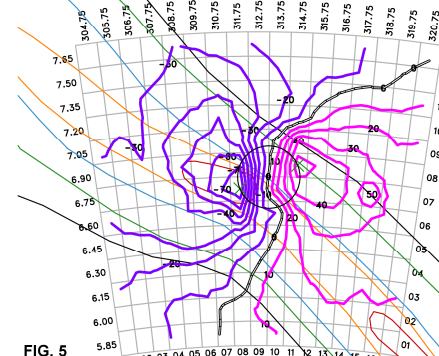


FIG. 5

20130520 $R_c = 5.4$ km, $AZ_c = 346.8^\circ$, $EL = 0.50^\circ$, $Z_c = 0.049$ km
 2017:01 UTC EFO E F2 E F4
 $V_{rot} = 77$ m s⁻¹ EF1 EF3 EF5
 $CD = 377$ m $V_{min} = -73$ $V_{max} = 81$

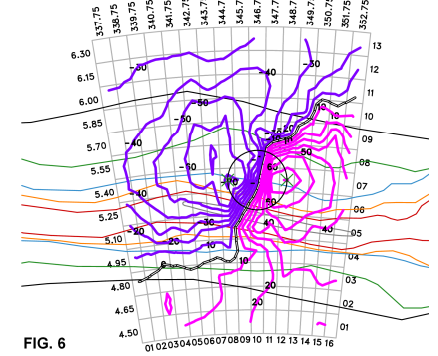


FIG. 6

FIG. 3. Same as FIG. 2, except for 1955:57 UTC. Date of data collection is indicated. Green X's represent extreme outbound and inbound Doppler velocity values across the estimated core diameter (CD, a black circle). The center range (R_c), azimuth (AZ_c), elevation angle (EL) and height (Z_c , AGL), shown at the top, represent the center grid (not necessarily equal to the signature grid center). The EF-ratings along the damage path are contoured according to different colors.

FIG. 4. Same as FIG. 3, except for 2005:53 UTC.

FIG. 5. Same as FIG. 3, except for 2009:58 UTC.

FIG. 6. Same as FIG. 3, except for 2017:01 UTC.

20130520 $R_c = 6.6$ km, $AZ_c = 11.8^\circ$, $EL = 0.50^\circ$, $Z_c = 0.060$ km
 2023:00 UTC EFO E F2 E F4
 $V_{rot} = 37$ m s⁻¹ EF1 EF3 EF5
 $CD = 360$ m $V_{min} = -42$ $V_{max} = 32$

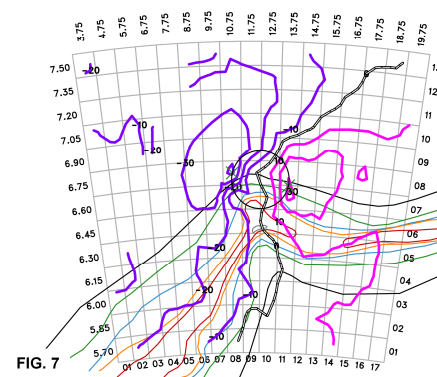


FIG. 7

FIG. 7. Same as FIG. 3, except for 2023:00 UTC.

20130520 $R_c = 7.3$ km, $AZ_c = 28.8^\circ$, $EL = 0.50^\circ$, $Z_c = 0.067$ km
 2025:55 UTC EFO E F2 E F4
 $V_{rot} = 40$ m s⁻¹ EF1 EF3 EF5
 $CD = 390$ m $V_{min} = -32$ $V_{max} = 48$

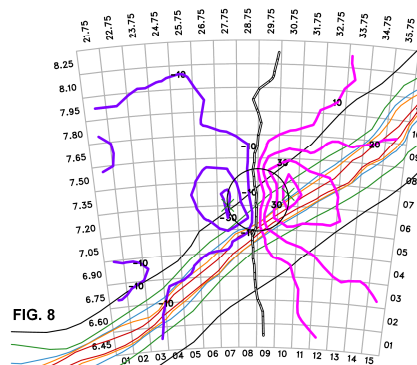


FIG. 8

FIG. 8. Same as FIG. 3, except for 2025:55 UTC.

20130520 $R_c = 9.8$ km, $AZ_c = 43.8^\circ$, $EL = 0.50^\circ$, $Z_c = 0.091$ km
 2029:34 UTC EFO E F2 E F4
 $V_{rot} = 45$ m s⁻¹ EF1 EF3 EF5
 $CD = 349$ m $V_{min} = -44$ $V_{max} = 46$

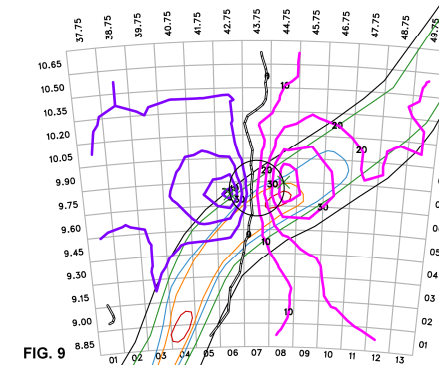


FIG. 9

FIG. 9. Same as FIG. 3, except for 2029:34 UTC.

20130520 $R_c = 12.1$ km, $AZ_c = 52.8^\circ$, $EL = 0.50^\circ$, $Z_c = 0.114$ km
 2035:00 UTC EFO E F2 E F4
 $V_{rot} = 31$ m s⁻¹ EF1 EF3 EF5
 $CD = 213$ m $V_{min} = -29$ $V_{max} = 34$

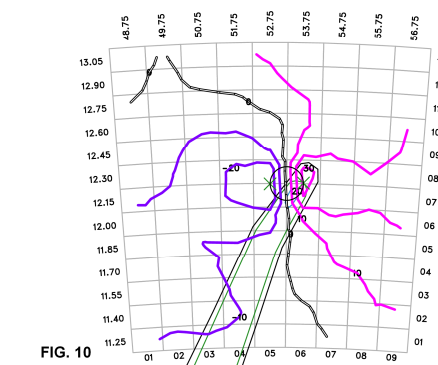


FIG. 10

FIG. 10. Same as FIG. 3, except for 2035:00 UTC.

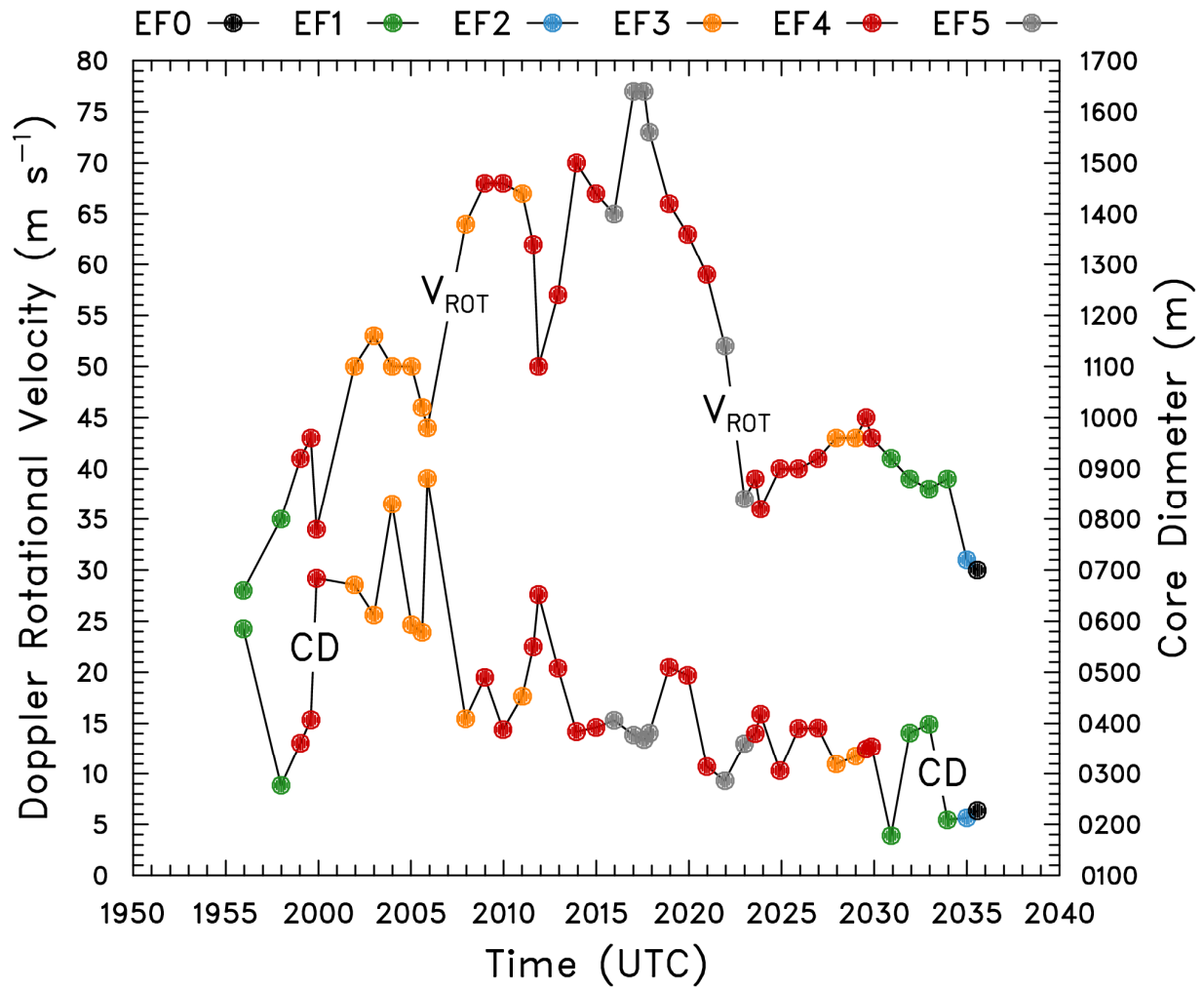


FIG. 11. Evolution of Doppler rotational velocity (V_{ROT}) and core diameter (CD) in relation to the varying (colored circles) EF ratings.